Emergence of superconductivity in mixture of nonsuperconducting ceramics La_2CuO_4 and $La_{1.56}Sr_{0.44}CuO_4$

A.A. Bykov[1*], K.Yu. Terent'ev[2], D.M. Gokhfeld[2, 3], N.E. Savitskaya[1], S.I. Popkov[2, 3], M.I. Petrov[2]
[1]Petersburg Nuclear Physics Institute named by B.P. Konstantinov of National Research Centre «Kurchatov Institute», 188300 Russia Gatchina, 1, mkr. Orlova roshcha
[2]Kirensky Institute of Physics, Federal Research Center KSC SB RAS, Krasnoyarsk, 660036 Russia
[3]Siberian Federal University, Krasnoyarsk, 660041 Russia
[*]E-mail: redi87@bk.ru

Abstract.

Composite materials fabricated by annealing of nonsuperconducting ceramics La_2CuO_4 and $La_{1.56}Sr_{0.44}CuO_4$ at 910° C during various time are investigated. Areas of superconducting $La_{1.85}Sr_{0.15}CuO_4$ phase arises at boundaries of contacting nonsuperconducting granules. The volume fraction of the superconducting phase increases with increasing the annealing time. A model describing the magnetic and transport properties of the samples at low magnetic fields is constructed. The magnetotransport characteristics of obtained samples at low magnetic fields (~ 100 Oe) are defined by a weak links network formed by superconducting areas. At high fields behavior of the system is defined by a magnetization of the disconnected superconducting islands. The average size of the superconducting areas has been estimated from an extended critical state model.

Keywords: magnetic properties, superconductivity, oxide superconductors, grain boundaries, LCO, LSCO, Josephson media

1. Introduction

The classical superconductor $La_{2-x}Sr_xCuO_4$ (LSCO) is studied since 1986. Its concentration phase diagram is known in the entire range of x [1]. La_2CuO_4 (LCO) is a weak ferromagnetic with a Neel temperature T_N = 500 K and it is dielectric. At $x > 0.25$, $La_{2-x}Sr_xCuO_4$ is a nonsuperconducting metal.

Recently [2,3], it was shown that an interface superconductivity arises on the boundary of LCO and $La_{1.56}Sr_{0.44}CuO_4$ films. Study of such films is limited by the complexity of their synthesis (a layer-by-layer molecular beam epitaxy). A solid-phase synthesis does not require the complicated tools and is a simple method for obtaining superconducting materials with a different size of grains. In a mixture of the over- and under-doped precursors, the diffusion of doping atoms at boundaries between the granules occurs. The diffusion and parameters of the superconducting phase can be controlled by the annealing time t_a.

In this paper, we present the results of an experimental study of samples obtained by annealing the mixture of LCO and $La_{1.56}Sr_{0.44}CuO_4$ ceramic powders. The synthesis of samples and the measuring techniques is described in Section 2. Experimental results are discussed in Section 3. A model describing the transport and the magnetic properties of the network of weak links is introduced in Section 4. Conclusions are presented in Section 5.

2. Materials and methods

The ceramic precursors of La_2CuO_4 and $La_{1.56}Sr_{0.44}CuO_4$ were synthesized by the standard solid-phase synthesis technique [4]. In addition, we synthesized the optimal doped sample LCSO as a benchmark. Then, the LCO and $La_{1.56}Sr_{0.44}CuO_4$ powders were grounded in an agate mortar and mixed in 0.66 / 0.34 mass proportions. The selected proportion of the components would, with complete diffusion of the elements, compose the superconducting phase $La_{1.85}Sr_{0.15}CuO_4$. The mixture of LCO and $La_{1.56}Sr_{0.44}CuO_4$ were annealed at T = 910° C in a preheated oven. After annealing, for restoring an oxygen stoichiometry, the samples were slowly cooled with the same rate in an air atmosphere. The diffusion coefficient of oxygen in HTSC ceramics is tenfold higher than that of strontium cations [5]. Hence, this cooling almost did not affect the diffusion of strontium. A series of the samples was annealed during the time t_a = 2, 6, 20, 60, 200, 600, 2000, 6000, 20000 min.

Scanning electron microscopy of the samples was performed on microscope Hitachi TM 3000. Temperature dependencies of the resistance $R(T)$ were measured by four-probe method by using QDS device of PPMS-6000. Samples with the parallelepiped form had dimensions of about $1\times1\times10$ mm^3. Transport current was equal to 1 mA. The temperature dependencies of the magnetization $M(T)$ and the magnetic field dependencies of the magnetization $M(H)$ were performed by using QD PPMS-6000 magnetometer.

3. Results and discussion

Fig. 1 shows microphotographs of samples with t_a = 2 and 2000 min. All the samples consist from irregular granules. The average granule size are estimated from microphotographs as 1.1±0.1, 1.2±0.1, 1.3±0.1 μm for t_a = 20, 200, 2000 min.

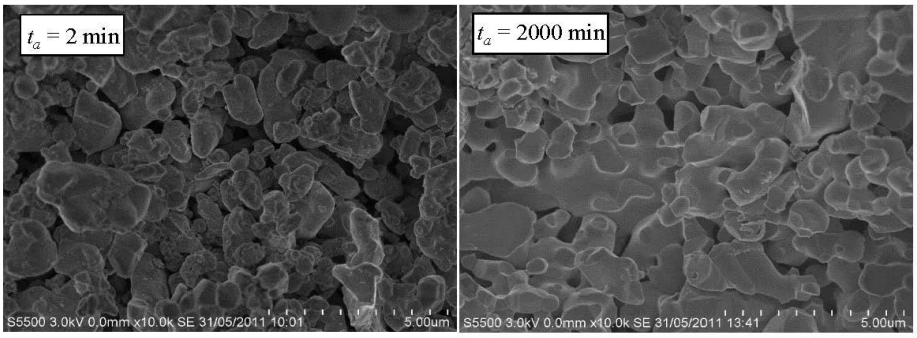

Fig. 1. Microphotographs of the samples with the annealing time t_a = 2 and 2000 min.

Fig. 2a shows temperature dependencies of the resistance of samples with different annealing times. All samples demonstrate a resistance jump at T_c = 37.5 K, the critical temperature of the optimally doped LSCO. For the samples with t_a = 6 and 20 min the resistance reaches the minimum at $T < T_c$ and then grows as temperature decreases. For the samples with longer t_a the resistance decreases at $T < T_c$ with decreasing temperature. Only for the sample with t_a = 20000 min the $R(T)$ curve reaches R = 0. At any fixed temperature the resistance decreases as the annealing time t_a increases. These facts indicate that there is the optimally doped LSCO in the samples and the volume fraction of the superconducting phase in the samples increases with t_a.

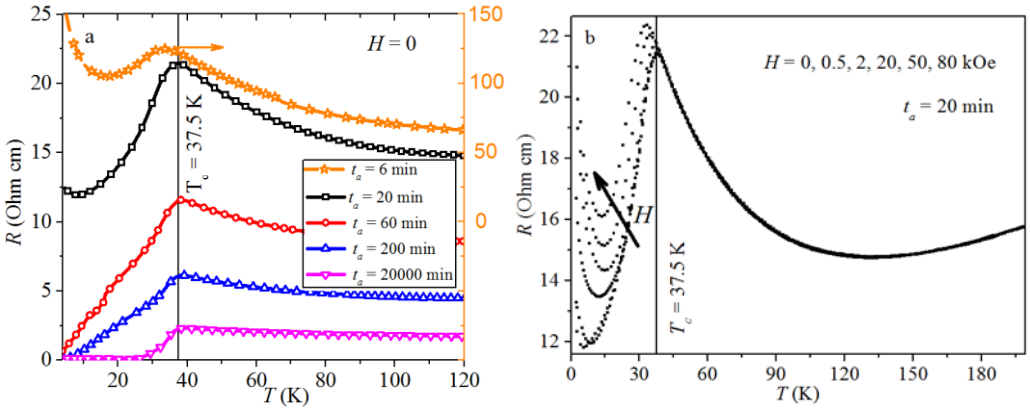

Fig. 2. Temperature dependencies of the resistance of samples with different annealing time t_a (a) and the dependencies for t_a = 20 min in magnetic fields (b).

Fig. 2b demonstrates temperature dependencies of the resistance for the sample with t_a = 20 min in various external magnetic fields. Influence of the magnetic field on the resistance of the samples is clearly pronounced in Fig. 3. It shows the dependencies of the additional resistance $\Delta R(T) = R(T, H) - R(T, H = 0)$. In high fields ($H$ = 20, 80 kOe) the $\Delta R(T)$ dependencies have a knee. This knee shifts to lower temperatures as the field is increased. These dependencies look similar to the $\Delta R(T)$ dependencies of polycrystalline superconducting composites [6-8] representing a network of Josephson weak links. For the composites the knee indicates that the superconductivity is suppressed in the surface of superconducting areas.

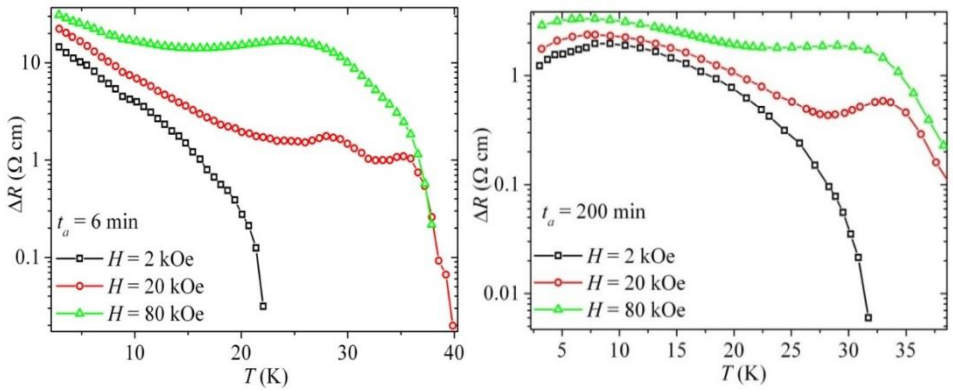

Fig. 3. Temperature dependencies of the additional resistance $\Delta R(T) = R(T, H) - R(T, H = 0)$ for t_a = 6 and 200 min.

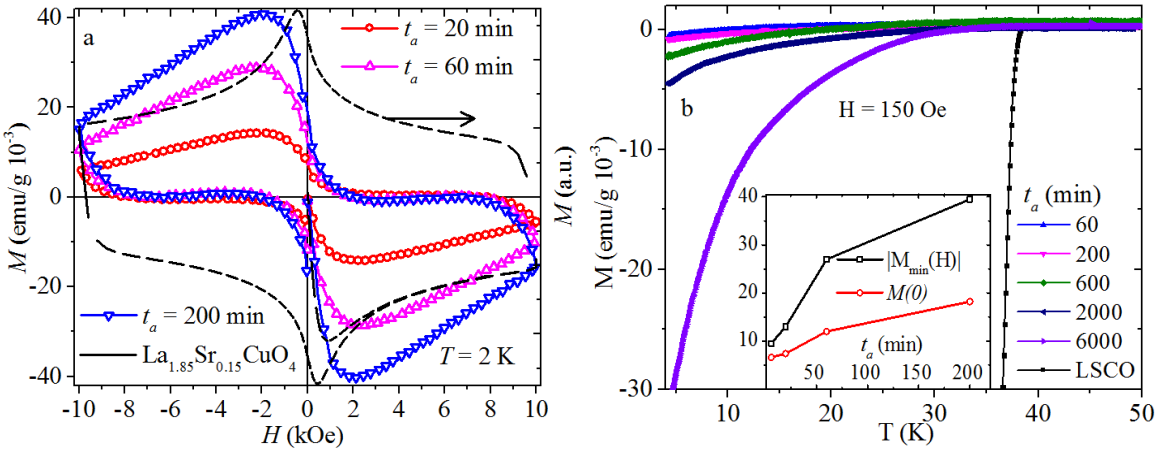

Fig. 4. Dependencies of the magnetization M on the magnetic field H (a) and temperature dependencies of the magnetization $M(T)$ in the ZFC regime (b). Insert shows the trapped field $M(0)$ and the absolute value of the magnetization minimum $|M_{min}|$.

Magnetization hysteresis curves of the samples are typical for HTSC. Also there is an additional paramagnetic contribution, which is apparently provided by the LCO granules. The $M(H)$ dependencies are shown on Fig. 4a (the paramagnetic contribution is subtracted for these loops). The $M(H)$ dependence of the optimally doped LSCO is also presented here. The magnetization loops of the samples are asymmetric relative to the M = 0 axis. Fig. 4b shows temperature dependencies of the magnetization $M(T)$ for some samples. The $M(T)$ dependencies tend to zero at T_c = 37.5 K. This, as well as the values of T_c obtained from $R(T)$, indicates that there is the optimally doped LSCO in the samples. The inset shows the dependencies of trapped field $M(0)$ and the minimum of the magnetization $|M_{min}|$ on t_a. The $M(0)$ and $|M_{min}|$ values, as well as magnetization width ΔM, depend on the volume of the superconducting phase. The observed growth of these parameters is supported to be due to the increasing of the superconducting volume fraction in the samples with t_a.

According to the extended critical state model (ECSM) [9, 10], an asymmetry of the magnetization loops and the trapped field $M(0)$ depend on the relation between the size of the current circulation d and the depth of the surface layer l_s. Also the critical current density J_c depends on the d/l_s ratio. From ESCM it follows that $J_c \approx J_{cb}(1 - 2l_s/d)^3$, where J_{cb} is the critical current density of the sample with $d >> l_s$ [11]. This relation allows us to estimate the d/l_s ratio from the observed asymmetry of magnetization loops. The critical current density J_c is given by the Bean formula $J_c = \Delta M/k$, where ΔM is the irreversible magnetization, $\Delta M = M_d - M_{up}$, $M_d(H)$ is the magnetization branch for the decreasing field, $M_{up}(H)$ is the magnetization branch for the increasing field, a parameter k is determined by the sample geometry and has the length dimension. For the polycrystalline sample one can use $k = d/3$ (in SI units) [12]. For the samples with $d >> l_s$, the

magnetization loop is symmetric relative to the $M = 0$ axis, and the irreversible magnetization ΔM equals $2|M_{up}|$ at the wide field range. Given $J_{cb} \approx (2|M_{up}|)/k$ we obtain $d/l_s \approx 2/ (1–(\Delta M/2|M_{up}|)^{1/3})$.

We assume that d corresponds to an average size of the superconducting areas in the investigated samples. Results of the estimations of d/l_s are presented in Table 1 for the values of ΔM and M_{up} at $H = 4000$ Oe. This field is about the full penetration field of the investigated samples.

t_a, min	d/l_s	I_c, μA
20000	-	18.5
200	8.6±0.8	3
60	8.5±0.7	2.2
20	9.0±0.9	2
6	10.7±1.3	1
LSCO	43.3±3.3	-

Table 1. Estimated parameters: the d/l_s ratio and the critical current I_c.

Given the average size of the benchmark LSCO granules to equal ~5-10 μm, the averaged island size d was supposed to be not higher than ~ 1 μm for all t_a. Assuming the value of l_s does not change with t_a, the size d is resulted to be independent of t_a within the errors. This is an unusual result because the volume fraction of the superconducting phase is found to grow with t_a.

Basing on experimental data we suppose that superconducting islands arise at boundaries of contacting granules as a result of strontium diffusion from over- to under-doped granules during the annealing. The stationary of the size d is an indirect confirmation of the diffusion mechanism of formation of the superconducting phase. When an over-doped granule contacts with an under-doped one, the impurities redistribute during the annealing. The redistribution forms a diffusion front [13] with the fixed depth. In this front, the strontium concentration is optimal for the superconducting phase. Before the front, the strontium concentration is insufficient, behind the concentration is exceeded. The depth of this front is resulted to be the size of the superconducting island.

We suggest that two superconducting subsystems [12] are segregated in the investigated samples. The first is superconducting islands emerged between granules with different Sr contents. The second is a network of weak links formed inside and between the superconducting areas. These subsystems demonstrate different behavior in magnetic fields and temperatures as well as for polycrystalline superconductors [6, 14]. At a low magnetic field (smaller than ~100 Oe), the critical current of the samples is defined by the weak links network. The thermally activated phase slippage model (TAPS) [15] is used to describe the long transition below T_c on the $R(T)$ dependencies of polycrystalline superconductors [16]. The average critical current I of weak links is used as the fitting parameter of TAPS. The TAPS curve for $I_c = 18.2 \pm 1.5$ μA coincides with the $R(T)$ dependence of the sample with $t_a = 20000$ min. The $R(T)$ dependencies of other samples are fitted worse. Agreement can be improved by taking into account i) the distribution function of the critical currents in weak links networks and ii) the temperature dependence of the resistance. By using approximate TAPS estimations of the averaged critical current without complicating accountings, we find that I_c grows with increasing t_a (Table 1).

At higher fields ($H > 100$ Oe) the weak links are resistive, and nondissipative supercurrents flow only into isolated superconducting islands. At H greater than ~10 kOe these islands contribute observably in the resistivity of the samples. It is because the magnetic field suppresses the superconductivity it the surface regions of the islands. The depth of the resistive surface region l_s grows as the magnetic field increases.

The number of the superconducting islands increases, as well as the critical current of the network, with increasing of the annealing time t_a. However, even at the longest t_a, total diffusion of strontium does not occur. The inner volume of the granules remains nonsuperconducting.

4. Theory

Now a model of the weak links network is described. This model gives the behavior of the samples in low fields (H ~ 100 Oe). We consider the two-dimensional task and do not account any temperature dependencies. Nonsuperconducting granules were placed in the cells of a disordered square lattice with size $N \times N$ on the x-y plane (Fig. 5a). The size of the granules along the z-axis is considered to be infinite. During annealing, granules contact better one to other and the superconducting areas emerge at the boundaries of the granules. The areas build a Josephson weak links network. In our model, the superconducting islands occur in some edges of cells. The shape of the superconducting areas is not important. We state that each superconducting area includes only one Josephson junction (Fig. 5b). Several weak links can occur on the superconducting area. But only the links with the minimal critical current determines the properties of superconducting circuits. Therefore this simplification does not affect the simulation of the electromagnetic properties of the network.

New superconducting edges are appeared during the annealing. These edges with Josephson junctions form closed contours around the normal phase clusters (Fig. 5c). Such the contours are the centers of pining for the magnetic flux. The number of the contours and their size distribution determine the electromagnetic properties of the whole system.

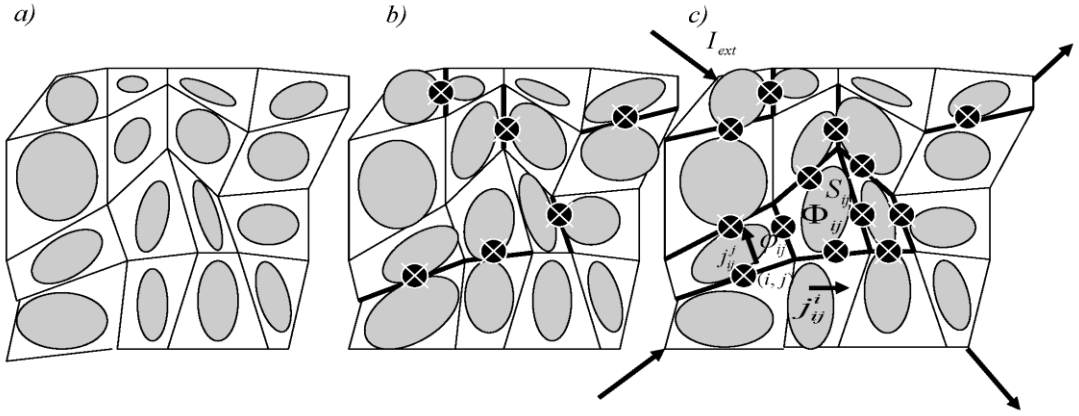

Fig. 5. The scheme of the weak links network formed by annealing. t_a increases from left to right, bold lines indicate the superconducting boundaries, crossed circles are the Josephson junctions.

Each Josephson junction is characterized by a dynamic variable, which is the gauge-invariant phase difference. Let us denote it as $\varphi_{i,j}$ for the junctions in the "vertical" edges of cells and $\theta_{i,j}$ for the "horizontal" ones (Fig. 5). The grid cells are numbered from the lower left corner. The density of the "vertical" and the "horizontal" currents, the cell area S_{ij} and the magnetic flux Φ_{ij} through the cell are given in Fig. 5 also. For $j^i_{i,j}$ and $j^i_{i,j}$, a discrete analog of Maxwell's equations is written (in the CGS electromagnetic system of units):

$$4\pi j^i_{i,j} = \frac{H_{i,j} - H_{i,j-1}}{d};\ 4\pi j^i_{i,1} = \frac{H_{i,1} - H_{ext}}{d};\ 4\pi j^i_{i,N} = \frac{H_{ext} - H_{i,N-1}}{d}$$

$$4\pi j^j_{i,j} = \frac{H_{i,j-1} - H_{i,j}}{d};\ 4\pi j^j_{1,j} = \frac{H_{ext} - H_{1,j}}{d};\ 4\pi j^j_{N,j} = \frac{H_{N-1,j} - H_{ext}}{d} \quad (1),$$

where $H_{i,j}$ is the magnetic field in the ij-th cell of the system, d is the length of the cell edge. This length is equal to the average size of the superconducting islands that is estimated above. From the resistive model of the Josephson junction [17], the junction current consists of normal and superconducting components:

$$j^i_{i,j} = \frac{\Phi_0}{2\pi r}\frac{d\theta_{i,j}}{dt} + j^i_{ci,j}\sin\theta_{i,j}$$

$$j^j_{i,j} = \frac{\Phi_0}{2\pi r}\frac{d\varphi_{i,j}}{dt} + j^i_{ci,j}\sin\varphi_{i,j} \quad (2),$$

where r is the normal resistance of the junction and $j^{i(j)}_{ci,j}$ is its critical current density. The magnetic

flux through the cell is expressed as [18]:

$$\Phi_{i,j} = \frac{\Phi_0}{2\pi}(\varphi_{i,j} + \theta_{i,j+1} - \varphi_{i+1,j} - \theta_{i,j}) \quad (3)$$

Combining (1) - (3), we obtain a system of equations for $\varphi_{i,j}$ and $\theta_{i,j}$ in the dimensionless form [19]:

$$\tau\frac{d\theta_{i,j}}{dt} + V\sin\theta_{i,j} = s_{i,j}(\varphi_{i,j} + \theta_{i,j+1} - \varphi_{i+1,j} - \theta_{i,j}) - s_{i,j-1}(\varphi_{i,j-1} + \theta_{i,j} - \varphi_{i+1,j-1} - \theta_{i,j-1})$$

$$\tau\frac{d\varphi_{i,j}}{dt} + V\sin\varphi_{i,j} = s_{i,j-1}(\varphi_{i,j-1} + \theta_{i,j} - \varphi_{i+1,j-1} - \theta_{i,j-1}) - s_{i,j}(\varphi_{i,j} + \theta_{i,j+1} - \varphi_{i+1,j} - \theta_{i,j})$$

$$\tau = \frac{4\pi < S_{ij} > d}{r};\ V = \frac{8\pi^2 d < S_{ij} > j_{ci,j}^{i(j)}}{\Phi_0};\ s_{i,j} = \frac{< S_{i,j} >}{S_{i,j}};\ (4)$$

where Φ_0 is the magnetic flux quantum and $S_{i,j}$ is the area of the cell. For the boundary junctions, according to (1), $H_{i,j}$ is replaced by H_{ext} in (4). For example, at the upper boundary, it is resulted in

$$\tau\frac{d\theta_{1,j}}{dt} + V\sin\theta_{1,j} = s_{1,j}(\varphi_{1,j} + \theta_{1,j+1} - \varphi_{2,j} - \theta_{1,j}) - 2\pi h_{ext};\ h_{ext} = \frac{H_{ext} < S_{i,j} >}{\Phi_0} \quad (5)$$

The system parameter $V_{i,j}^{i(j)}$ depends on the critical current of the junctions. This value concerns to a number of magnetic vortices in the corresponding contour. If some edge of cells does not contain the superconducting island and the Josephson junction then its critical current and the quantity $V_{i,j}^{i(j)}$ are equal to zero. When all $V_{i,j}^{i(j)} \gg 1$, the system has a large number of metastable energy states. Consequently, the network demonstrates the hysteresis magnetic behavior. In the contrary case of all $V_{i,j}^{i(j)} \ll 1$, the magnetic dynamics of the network is reversible [18]. Using estimated values of d and I_c, the averaged <V> is found to be ~40.

In our model, we take into account the changes that occur with the sample during the annealing. Initially, all the granules are considered to be not touched one to other and all values $V_{i,j}^{i(j)}$ equal zero. As t_a increases, the granules begin to touch some nearest neighbors. The edge of the lattice cell, along which the granules come into contact, becomes superconducting. We introduce the quantity a determining the probability of arising of the new superconducting edges during the time cycle. Then the number of the superconducting edges is determined by t_a and a. During annealing, the amount of the superconducting edges increases and the closed superconducting contours are formed. The normal clusters surrounded by the superconducting contours are the pinning centers. The results of 21 x 21 lattice modeling for the probability a = 0.01 are presented in Fig. 6. It is seen that, the pinning centers in the system are added as t_a increases.

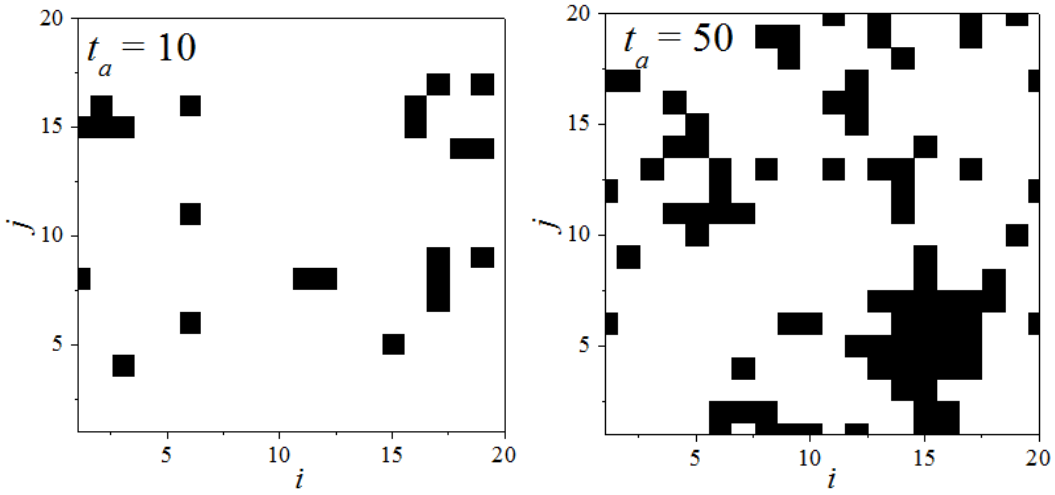

Fig. 6. Simulation results. Black sections denote pinning centers (the normal clusters, surrounded by the closed superconducting contour).

We simulate the behavior of the annealed sample in two modes. The first correspond to the external magnetic field $H_{ext}(t)$ applied along the z-axis of the sample. The second correspond to the direct current I_{ext} along the x-axis of the sample. In this geometry, the demagnetization factor can be neglected.

In the first case, the critical current density depends on magnetic field as $j_{ci,j}^{i(j)} = j_{0i,j}^{i(j)}/(1+H_{i,j}/H_0)$. The values of $j_{0i,j}^{i(j)}$ are chosen to obtain ($V_{i,j}^{i(j)} \geq 40$). It does not matter whether the critical currents of all the junctions are different or identical. The electromagnetic properties of the system are determined only by the mean value of the critical current. The external field is changed so that its dimensionless value is added by one $h_{ext} \rightarrow h_{ext}+1$ during the computational cycle. This field growth is assumed to be so slow that all the processes in the system could be completed before the next cycle. For each value of the external field, we calculate the dimensionless mean value of the magnetic field inside the sample and the magnetization:

$$b = \frac{1}{N^2}\sum_{i,j}\frac{\Phi_{i,j}}{\Phi_0}s_{i,j}; \quad (5)$$

$$M = \frac{1}{4\pi}(b - h_{ext})$$

As a result, the magnetization loops for various t_a were computed (Fig. 7a). Here the cell areas are chosen to be the same and, consequently, $S_{i,j} = 1$ for all cells of the system. It is seen that the trapped magnetic flux increases with t_a as well as the $M(0)$ values. This result qualitatively agrees with the experiments. The shape of the hysteresis loop is affected by the value of H_0, which depends on the material.

In the second case, a direct current I_{ext} flow through the network without external magnetic field. We assume that the current is injected into the "horizontal" contacts of the upper and lower boundaries of the system (Fig. 5c). Then, the boundary conditions of (4) are changed. At the upper and lower boundaries, the external magnetic field is replaced by $i_{ext} = I_{ext}dS/\Phi_0$. At the right and left boundaries, the external field is replaced by zero. Now $j_{ci,j}^{i(j)}$ is considered to be independent of the local magnetic field. The values of $j_{ci,j}^{i(j)} = j_c$ are chosen to have V = 40. Further, the average voltage for horizontal contacts was calculated for various I_{ext} by the formula:

$$u^i = \frac{1}{N(N-1)}\frac{2\pi}{\Phi_0}\sum_{i,j}u_{i,j}^i$$

$$u_{i,j}^i = \frac{\Phi_0}{2\pi}\frac{d\theta_{i,j}}{dt}$$

The $u^i(2\pi i_{ext}/V)$ dependencies for different t_a are presented in Fig. 7b. It is seen that for higher t_a, the voltage-current curve is closer to the curve of a superconductor with $j_c = V/2\pi$. The increase of $j_{ci,j}^{i(j)}$ is caused by the increasing number of the superconducting contours, which are able to carry the corresponding critical current.

The dependence of the resistance on the external magnetic field $R(H)$ is computed also (Fig. 7c). The external current $i_{ext} = 0.9(V/2\pi)$ flow through the sample according to the scheme in Fig. 5c. The dependence of j_c on the external magnetic field is given by $j_c = j_{c0}/(1+H_{ij}/H_0)$ with $H_0 = 2$. Fig. 7c shows, the resistance of all samples increases with h until the critical field of weak links. The critical field of weak links depends on the parameter H_0. It is also seen that the resistance decreases with increasing t_a. The computed $R(H)$ dependencies qualitatively coincide with experimental curves of polycrystalline superconductors in low fields [6-8].

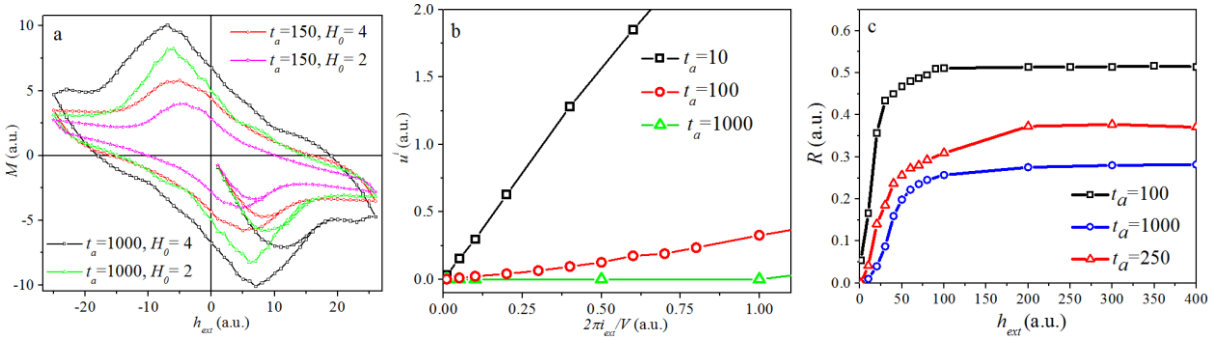

Fig. 7. Computed curves for some t_a: magnetization loops with different H_0 (a), *I-V* curves (b), the resistance *R* versus the external magnetic field *H* (c).

5. Conclusions

Annealing the mixture of powders of nonsuperconducting ceramics La_2CuO_4 and $La_{1.56}Sr_{0.44}CuO_4$ we have obtained the composite samples owning superconducting properties. From the results of experimental investigations and numerical simulating we can conclude:

1. The volume fraction of the superconducting phase increases with annealing time t_a. However, even at the longest t_a, the fraction of superconducting phase is smaller than 50 %. Consequently, complete diffusion of strontium does not occur. The superconducting phase in the samples is the islands of LSCO at the boundaries of the contacting over- and under- doped granules. The inner bulk of the granules remains nonsuperconducting.

2. The behavior of the samples in low (< 100 Oe) magnetic fields is determined by the properties of the weak links network. At high magnetic field, the superconductivity of weak links is destroyed. Then the behavior of the system is determined by separate LSCO islands. Superconductivity is suppressed by magnetic field in the surface regions of the superconducting islands. This contribution to resistance is significant at magnetic fields higher than 10 kOe.

3. The extended critical state model is used to estimate the average size *d* of the superconducting islands. It is shown that *d* does not depend on t_a. This confirms the diffusion formation of the superconducting islands.

4. The model of the magnetic and transport behavior of the samples in low magnetic fields is presented. The model adequately describes the observed physical properties of the samples. In addition, the model predicts the possibility to discover some new interesting phenomena that can realize in our system, for example, self-organized criticality [19].

Acknowledgements

The authors are grateful to D.A. Balaev for fruitful discussions, and I.V. Nemtsev for electronic microscope measurements in the center for shared use, KSC SB RAS. The work is supported by the Russian Science Foundation (project No. 17-72-10067).

Literature

[1] N. Plakida, High-Temperature Cuprate Superconductors, Springer Berlin Heidelberg, Berlin, Heidelberg, 2010. doi:10.1007/978-3-642-12633-8.

[2] G. Logvenov, A. Gozar, I. Bozovic. High-Temperature Superconductivity in a Single Copper-Oxygen Plane // *Science* 326, 699–702 (2009);

[3] T. Misawa, Y. Nomura, S. Biermann, M. Imada, Self-optimized superconductivity attainable by interlayer phase separation at cuprate interfaces, Sci. Adv. 2 (2016) e1600664. doi:10.1126/sciadv.1600664.

[4] A.G. Mamalis, S.G. Ovchinnikov, M.I. Petrov, D.A. Balaev, K.A. Shaihutdinov, D.M. Gohfeld, S.A. Kharlamova, I.N. Vottea, Composite materials on high-Tc superconductors and BaPbO3, Ag basis, Phys. C Supercond. Its Appl. 364–365 (2001) 174–177. doi:https://doi.org/10.1016/S0921-4534(01)00749-3.

[5] T.D. Dzhafrov, Diffusion in High-Temperature Superconductors, Phys. Status Solidi. 158

(1996) 335–358. doi:10.1002/pssa.2211580202.
[6] D.A. Balaev, D.M. Gohfeld, S.I. Popkov, K.A. Saihutdinov, M.I. Petrov, High-temperature superconductor based composites: Large magnetoresistance in weak magnetic fields, Tech. Phys. Lett. 27 (2001) 952–955. doi:10.1134/1.1424404.
[7] D.A. Balaev, A.G. Prus, K.A. Shaykhutdinov, D.M. Gokhfeld, M.I. Petrov, Study of dependence upon the magnetic field and transport current of the magnetoresistive effect in YBCO-based bulk composites, Supercond. Sci. Technol. 20 (2007) 495, doi: 10.1088/0953-2048/20/6/002.
[8] D.A. Balaev, A.A. Bykov, S. V. Semenov, S.I. Popkov, A.A. Dubrovskii, K.A. Shaikhutdinov, M.I. Petrov, General regularities of magnetoresistive effects in the polycrystalline yttrium and bismuth high-temperature superconductor systems, Phys. Solid State. 53 (2011) 922–932. doi:10.1134/S1063783411050052.
[9] D.M. Gokhfeld, D.A. Balaev, M.I. Petrov, S.I. Popkov, K.A. Shaykhutdinov, V. V. Valkov, Magnetization asymmetry of type-II superconductors in high magnetic fields, J. Appl. Phys. 109 (2011) 33904. doi:10.1063/1.3544038.
[10] D.M. Gokhfeld, An extended critical state model: Asymmetric magnetization loops and field dependence of the critical current of superconductors, Phys. Solid State. 56 (2014) 2380–2386. doi:10.1134/S1063783414120129.
[11] D. Gokhfeld, Critical current density and trapped field in HTS with asymmetric magnetization loops, J. Phys. Conf. Ser. 695 (2016) 12008. doi:10.1088/1742-6596/695/1/012008.
[12] S. Senoussi, Review of the critical current densities and magnetic irreversibilities in high T c superconductors, J. Phys. III. 2 (1992) 1041–1257. doi:10.1051/jp3:1992102.
[13] K. Hauffe, Reaktionen in und an Festen Stoffen, Springer Berlin Heidelberg, Berlin, Heidelberg, 1955. doi:10.1007/978-3-642-52680-0.
[14] I.L. Landau, J.B. Willems, J. Hulliger, Detailed magnetization study of superconducting properties of $YBa_2Cu_3O_{7-x}$ ceramic spheres, J. Phys. Condens. Matter. 20 (2008) 95222. doi:10.1088/0953-8984/20/9/095222.
[15] V. Ambegaokar, B.I. Halperin, Voltage Due to Thermal Noise in the dc Josephson Effect, Phys. Rev. Lett. 22 (1969) 1364–1366. doi:10.1103/PhysRevLett.22.1364.
[16] D.A. Balaev, S.I. Popkov, K.A. Shaihutdinov, M.I. Petrov, Physica C 435 (2006) 12–15.
[17] A. Barone, G. Paterno, Physics and applications of the Josephson effect, New York, Wiley 1982, DOI: 10.1002/352760278X.
[18] D.-X. Chen, J.J. Moreno, A. Hernando, Evolution from the vortex state to the critical state in a square-columnar Josephson-junction array, Phys. Rev. B. 53 (1996) 6579–6584. doi:10.1103/PhysRevB.53.6579.
[19] S.L. Ginzburg, A. V Nakin, N.E. Savitskaya, Avalanche dynamics of magnetic flux in a two-dimensional discrete superconductor, J. Exp. Theor. Phys. 103 (2006) 747–755. doi:10.1134/S1063776106110100.